Report SCEC Proposal 21154

Is topography part of the "key" in the Cajon Pass earthquake gate? Continuing study with realistic and synthetic models.

Christodoulos Kyriakopoulos
Center for Earthquake Research and Information, University of Memphis

David D. Oglesby (not funded in this proposal)
Earth and Planetary Sciences, University of California, Riverside

Amount of Request: $33,463;

Amount of Funded: $15,000;

Proposal Category: B

SCEC Research Priorities / Science Objectives: 4a, 1e, 2e

Start Date: February 1, 2021

1.Background and motivation

This work is a continuation of the previously supported SCEC project #19223 and #20151 and investigates the effect that topographic asymmetry has on the rupture propagation across the Cajon Pass (CP) in Southern California. Our investigation is based on the use of 3D dynamic rupture models. We designed experiments that allow us to compare results between models with topography (realistic and synthetic) and models with a flat free surface. Although our work is focused on the Cajon Pass area, additional synthetic models allow us to draw more general conclusions that are applicable to other areas of the world and topographic effects in general. Part of out the findings regarding subshear ruptures (S=2.0) and interaction with asymmetric topography have been published in:

Kyriakopoulos, C., Wu, B., & Oglesby, D. D. (2021). Asymmetric topography causes normal stress perturbations at the rupture front: The case of the Cajon Pass. Geophysical Research Letters, 48, e2021GL095397. https://doi.org/10.1029/2021GL095397

A second paper discussing supershear (S<=1.0) ruptures is under preparation. The effect of topography on ground motion and particularly amplification effects has been documented in recent publications (e.g., Bouchon, 1973, Trifunac, 1973, Wong, 1982, Geli et al., 1988, Bouchon et al., 1996, Ma et al., 2007). Most previous investigations are focused on propagating wave fronts and interaction with the irregular topographic surface (mountains and valleys). However, they do not explore the effect of topographic surface on the propagating rupture front. In that prospective a limited number of studies exist, and their results imply that, in some cases, the effect of scattered reflections off the topography can have a significant effect on rupture propagation, specifically slip-rate and slip (Ely et al., 2010, Kyriakopoulos et al. 2017, Zhang et al., 2015). In the specific case of the Cajon Pass (Figure 1), its geographic location is thought to modulate and control the generation of large earthquakes in southern California (SoCAL) behaving essentially as an "Earthquake Gate" (EG). The mechanism for which the CP serves as an EG are net yet understood. An obvious question is whether the topographic relief surrounding the CP could have an effect to this "gate-like" behavior. In southern California the San Andreas fault traverses or borders several

topographic features that include deserts and high mountain relies. Near the CP, the fault extends from the flat Coachella Valley to the base of the San Bernardino Mountains (3000+ m), runs through the CP and up into the San Gabriel Mountains, where it reaches an elevation of around 2000 m before descending to the Mojave Desert.

We specifically investigated the following topics:

1) Super shear ruptures with asymmetric topography
2) Permanent (static) normal stress changes
3) Effect of shallower locking depth
4) Effect of absolute stress and near surface stress ramp

2.Method

Our investigation of the topographic asymmetry is based on dynamic rupture simulations using four (4) different 3D finite element models. More specifically, a "topographic" model implementing a downsampled version of the realistic topography of southern California (Figure 1A), a "flat" model implementing a flat surface (Figure 1B), a "synthetic" topographic model (Figure 1C and 1D) implementing an idealized synthetic version of the topographic asymmetry observed around the CP and its flat counterpart (not shown

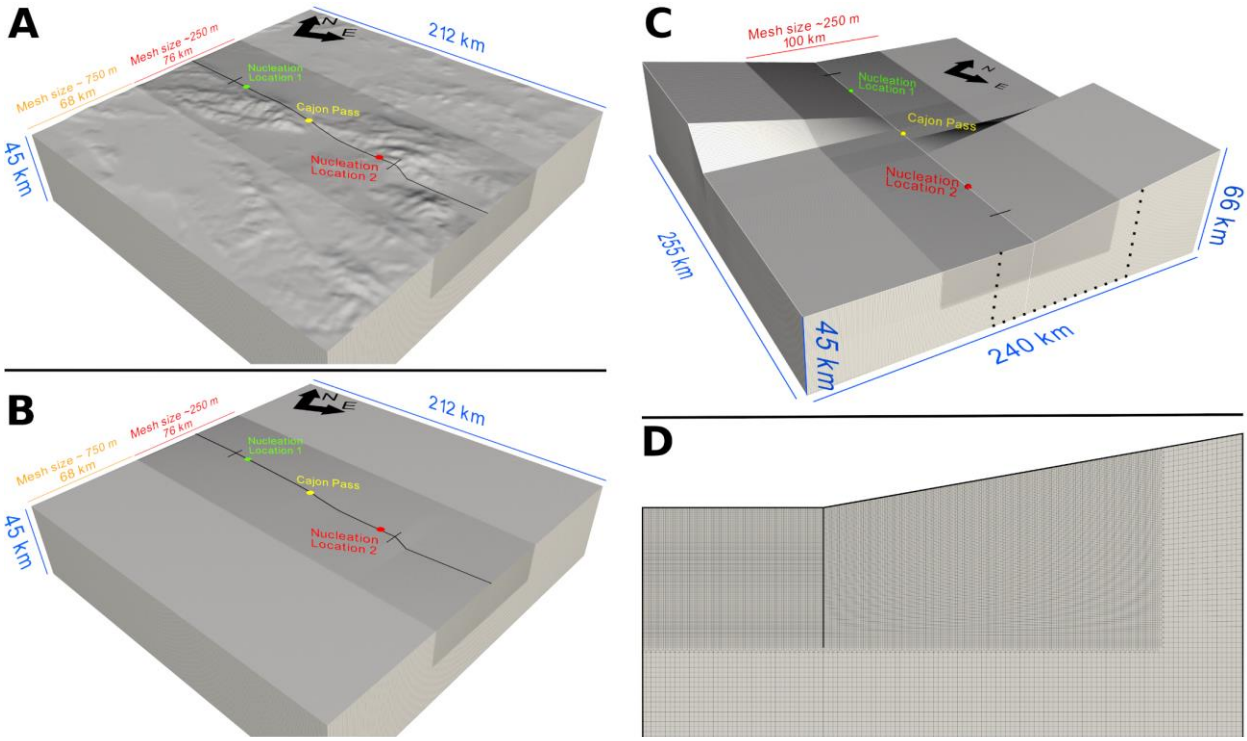

Figure 1. Models used in this work. *Comparison between (A) "Topographic" and (B) "Flat" free surface mesh. (C) "Synthetic" topographic model and (D) mesh detail from lateral view. The two nucleation locations, north and south of the Cajon Pass, are marked with a green (Nucleation location 1) and a red (Nucleation location 2) disc, respectively. The Cajon Pass is shown with a yellow disc. The dotted line in (C) highlights the lateral area shown in panel (D). The black arrows point to the north and east directions. The long black line in (A) and (B) represents the UCERF3 fault line implemented in our models. The two black lines perpendicular to the fault line shown in (A), (B) and (C) mark the rupturable length.*

here) named the "synthetic flat". Both the "topographic" and "flat" models implement a fault geometry of the southern portion of the San Andreas fault based on UCERF3 (Field et al., 2013), with its vertical dip and several bends along strike. The "synthetic" topographic and "synthetic flat" models implement a

vertical fault with no along-strike bends. Although normal stress does not change along vertical planar faults in a half-space, normal stress variations are observed in our experiments due to the along-strike (bending) change in geometry. For thar reason the experiments with the synthetic model (without along-strike bends) are crucial in isolating the asymmetric topography effects without the effect of normal stress changes caused by fault bending. All models are generated using the meshing code Trelis (coreform.com) and further details regarding the mesh are presented in *Kyriakopoulos et al., 2021* and supplementary materials. To run our dynamic rupture models, we use the code FaultMod (Barall, 2009), tested in the SCEC community benchmark exercise (Harris et al., 2009). The allowed rupture length is approximately 120 km along strike, with a 15 km locking depth. To isolate the first order effects of the topographic surface we use homogeneous material properties with a Poisson ratio of 0.25, a V_P of 5477 m/s, and a V_S of 3162 m/s. We use slip-weakening friction (Ida, 1972; Andrews, 1976) with a static frictional value of 0.6, a sliding frictional value of 0.1, and a slip weakening distance of 0.3 m. Decisions on prestress conditions are made using the fault strength parameter $S = \frac{\tau_{yield} - \tau_{initial}}{\tau_{initial} - \tau_{final}}$ (Andrews et al., 1976), using values of S=0.45, S=1 and S=2. Lower S values indicate a system more favorable to rupture while higher S values indicate the opposite. We experimented with S=0.45 (Burridge–Andrews supershear mechanism), S=1.0 (super shear jump induced by the free surface; Kaneko and Lapusta, 2010), and S=2.0 where rupture travels at sub-Rayleigh speeds. However, our first paper (Kyriakopoulos et al., 2021) discusses the subshear case and we left the discussion regarding supershear ruptures and permanent static effects to be included in future manuscripts. Ruptures are driven across the CP using two nucleation locations at ~50km north of the CP and ~50km south of the CP. Real earthquakes in this area could easily span a larger portion of the SSAF than our fault model, and for that reason our simulations should not be taken as an indication of maximum earthquake size.

3.Discussions on the effect of absolute stress and stress reduction near the free surface

During the last year of project #21154 new questions arose regarding the effect of absolute stress level and the effect of near surface stress reduction. We generated a new set of simulations with a progressive reduction in stress above 3 km depth, such that the shear and normal stresses are reduced to 1/10 their ambient values at the free surface (see Figure S3 in Kyriakopoulos et al., 2021). Results with constant stress with depth are also presented in the supplementary materials of the same paper (Figure S4, S5). To investigate the effects of absolute stress on our models, we also perform models with a normal stress 5 times larger than our primary models, but with the same stress drop and S value (Figure S6, S7); these models have the same static friction as our primary models, but a higher sliding friction of 0.5 to allow the slips to be comparable. Our experiments with and without depth-dependent stress in the synthetic models indicate that the dynamic normal stress perturbations do not disappear in the presence of reduced initial stress near the Earth's surface. This result emphasizes that the dynamic normal stress perturbations are primarily determined by the fault slip, which while reduced at the free surface, is not reduced by 90% like the ambient stress. The lower the stress near the free surface, the more the normal stress perturbations will tend to dominate the on- and off-fault behavior at shallow depths. Our models with higher ambient stress show that the effects of surface topography are also not very sensitive to the overall effective stress level, producing similar amplitudes of stress perturbation. While the percentage change in stress is obviously lower for our high-stress model, we note that due to the higher frictional coefficient in this model, the feedback between shear and normal stress in the slipping region is also higher. Another end member for a high-stress model (not shown in the current work) is to have the same friction coefficients as the low stress case, but to scale the stress values up by some factor. In this case, the slip and the stress perturbation will scale up by approximately the same factor as the stress, leaving the relative importance of the stress perturbation unchanged from the low-stress case.

4.Permanent normal stress changes

The asymmetric topography effect although clearly visible during dynamic rupture it also leaves a residual (static) increment in normal stress. The permanent normal stress effect is particularly visible in the synthetic

topographic model because implements a vertical fault without along strike variations in (that does not include permanent stress changes due to bending). Figure 2 shows comparisons of final slip and permanent normal stress changes for the "synthetic" topographic and "synthetic flat" rupture models. Both models are pre-stressed at the S=1.0 level (free surface induced supershear transition). Figures 2A and 2C show the final slip distribution while Figures 2B and 2D show the final normal stress change. The final slip distribution is similar between the two cases, both models show a patch of higher slip near the center of the model. This pattern is determined by the free surface induced super shear transition. However, the models are significantly different if we observe the permanent normal stress change. Of particular interest is the concentration of normal stress increase in the CP in the topographic model. The flat model doesn't show any changes in normal stress as expected for a vertical fault. It is also interesting to note that the edges of the rupture area in the topographic model are also clamped, defining in that way two normal stress "barriers". Another interesting observation is that the permanent effect corresponds to the normal stress sign behind the rupture front. For that reason, the normal stress pattern reveals the direction of rupture (north-to-south in our model, left-to-right for the reader). In our current parametrization for the synthetic topographic model the normal stress changes are bounded between -0.5 and 0.5 MPa. Although these changes are lower than permanent changes associate with fault bending it is still interesting how the geometry of the fault system combined with the topography near the CP generates a normal stress concentration pattern. Experiments with nucleation on the CP (not shown here) confirm the permanent stress changes observed when nucleation is either south or north of the CP, although the normal stress pattern is symmetric with respect to the CP.

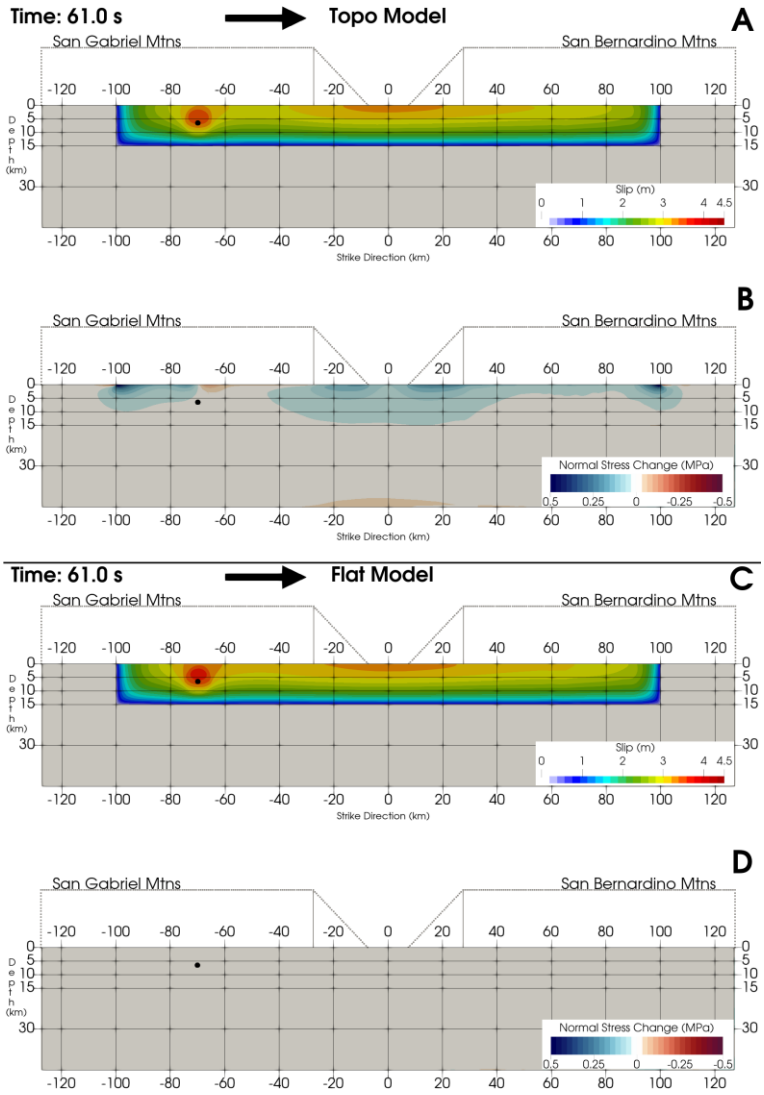

Figure 2. Permanent normal stress changes with and without topography. *(a) and (b) final slip distribution and permanent normal stress change around the CP observed in experiments with the "synthetic" topographic model. (c) and (d) final slip and permanent normal stress change for the "synthetic flat" model. Both models implement a vertical fault with no along-strike bends. A comparison between panels (b) and (d) highlights the effect of asymmetric topography on the final normal stress pattern.*

5.Effect of smaller locking depth

To explore the effect of a shallower locking depth we ran experiments where we decrease the locking depth from 15 to 10 km. Here we are discussing briefly experiments with the "synthetic" topographic model and values of S=2.0 and S1.0. Simulations with shallower locking depth confirm qualitatively all the previous

observations made with our original models for both the dynamic as well as the permanent static stress change near the CP. Because of the reduction in seismogenic width (locking), the models with shallower locking depth produce lower slip values and are consequently downscaled with respect to the previous models. Because the normal stress changes observed in our models depend on the slip intensity, both the dynamic and permanent stress changes observed in these new models are proportionally affected.

6. Discussion on supershear ruptures

To gain a better understanding of supershear ruptures with asymmetric topography we ran a series of models with the "synthetic" topographic and the "synthetic flat" models that both implement a vertical fault with no along-strike bends (Figure 3). These allow us to study the normal stress changes without the confounding effect of the along-strike bends present in the "topographic" and "flat" models that use the UCERF3 fault geometry. Compared to the subshear (S=2.0) case presented in *Kyriakopoulos et al., 2021*, the new set of experiments confirms all the previous findings while at the same moment generate new topics for discussion. We observe that the supershear normal stress topographic changes are caused by two separate rupture fronts, instead of one clamping-unclamping pattern observed in the subshear (S=2.0) case, the leading daughter rupture front (generated by the free-surface induced super-shear jump) and the trailing parent sub-Rayleigh front (Figure 3A and 3B). We can distinguish two separate concentrations of clamping-unclamping (red-blue - red-blue) ahead and behind each rupture front, and because of this separation, the normal stress perturbation is distributed over a larger area in the along-strike direction. During the later stages of rupture, and as the sub-Rayleigh front becomes weaker, the normal stress pattern appears to be the result of constructive and destructive interference between the two fronts. For that reason, is not easy to discern the original normal stress patterns of alternating clamping and unclamping. It is interesting to note that for an experiment with S=0.45 (Burridge–Andrews supershear mechanism; Figure 3C and 3D) we do not observe two separate concentrations of clamping-unclamping because the super shear jump occurs at depth. In both the S=1.0 and S=0.45 cases a Mach front is clearly evident on both the slip rate and normal stress pattern.

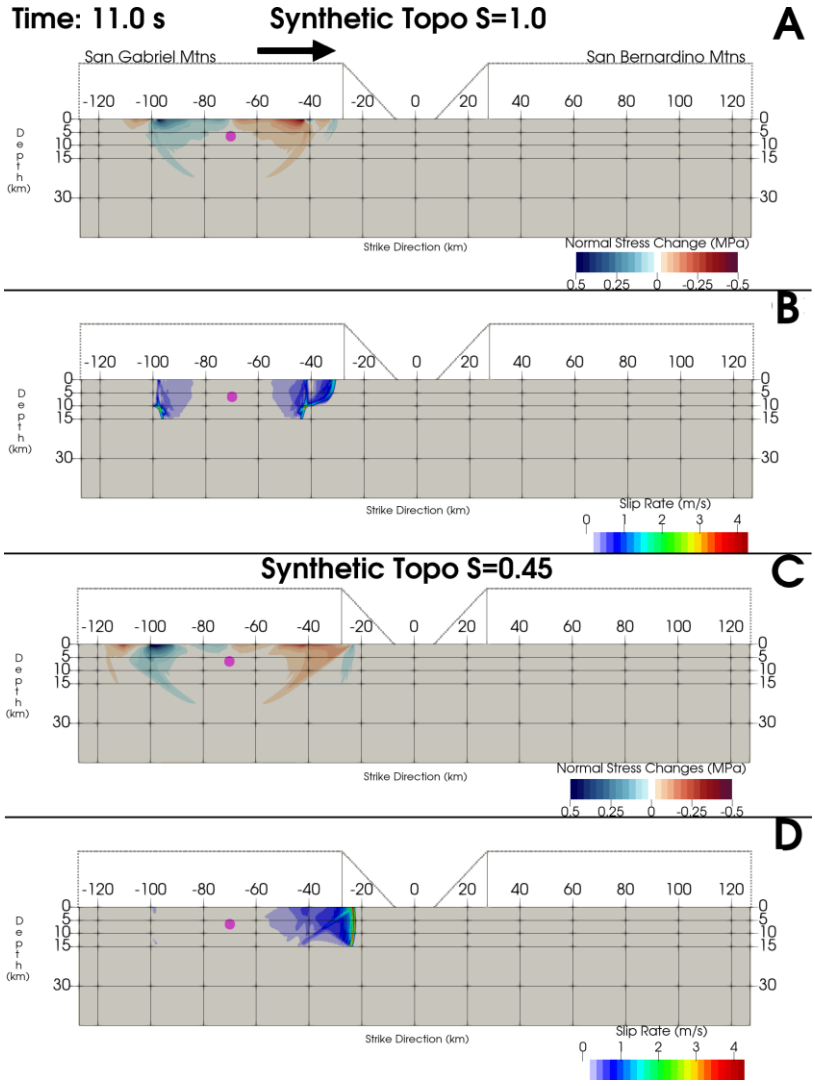

Figure 3. Time snapshot (t = 11 s) of super shear rupture using the "synthetic" topographic model and north-to-south propagation. *(a) normal stress perturbation and (b) slip rate around the CP observed in experiments with S=1.0 (free surface induced supershear). (c) and (d) same with the previous two panels although for an experiment with S=0.45 (classical Burridge–Andrews supershear). Both models implement a vertical fault with no along-strike bends.*

Bibliographic References

Bouchon, M., 1973. Effect of topography on surface motion, Bulletin of the Seismological Society of America, 63, 615-632.

Bouchon, M., Schultz, C.A. & Toksöz, M.N., 1996. Effect of three-dimensional topography on seismic motion, Journal of Geophysical Research, 101, 5835-5846.

Ely, G.P., Day, S.M. & Minster, J.-B., 2010. Dyanamic rupture models for the southern San Andreas fault, Bulletin of the Seismological Society of America, 100, 131-150.

Field, E.H., et al. (2013), Uniform California earthquake rupture forecast, version 3 (UCERF3)—The time-independent model: U.S. Geological Survey Open-File Report 2013–1165, 97 p., California Geological Survey Special Report 228, and Southern California Earthquake Center Publication 1792, http://pubs.usgs.gov/of/2013/1165/.

Geli, L., Bard, P.-Y. & Jullien, B., 1988. The effect of topography on earthquake ground motion: a review and new results, Bulletin of the Seismological Society of America, 78, 42-63.

Harris, R. A., Barall, M., Archuleta, R., Dunham, E., Aagaard, B., Ampuero, J. P., et al. (2009). The SCEC/USGS dynamic earthquakerupture code verification exercise. Seismological Research Letters, 80(1), 119–126. https://doi.org/10.1785/gssrl.80.1.119

Ida, Y. (1972). Cohesive force across the tip of a longitudinal-shear crack and Griffith's specific surface energy. Journal of Geophysical Research, 77(20), 3796-3805.

Kyriakopoulos, C., Wu, B., & Oglesby, D. D. (2021). Asymmetric topography causes normal stress perturbations at the rupture front: The case of the Cajon Pass. Geophysical Research Letters, 48, e2021GL095397. https://doi.org/10.1029/2021GL095397

Kyriakopoulos, C., Oglesby, D.D., Funning, G.J. & Ryan, K.J., 2017. Dynamic rupture modeling of the M7.2 2010 El Mayor-Cucapah earthquake: Comparison with a geodetic model, Journal of Geophysical Research, 122, 10,263-210,279.

Y. Kaneko and N. Lapusta (2010), Supershear transition due to a free surface in 3-D simulations of spontaneous dynamic rupture on vertical strike-slip faults, Tectonophysics, Volume 493, Issues 3–4, 2010, Pages 272-284, https://doi.org/10.1016/j.tecto.2010.06.015.

Ma, S., Archuleta, R.J. & Page, M.T., 2007. Effects of large-scale surface topography on ground motions, as demonstrated by a study of the San Gabriel Mountains, Los Angeles, California, Bulletin of the Seismological Society of America, 97, 2066-2079, doi:2010.1785/0120070040.

Trifunac, M.D., 1973. Scattering of plane SH waves by a semi-circular canyon, Earthquake Engineering and Structural Dynamics, 1, 267-281.

Wong, H.L., 1982. Effect of surface topography on the diffraction of P, SV, and Rayleigh waves, Bulletin of the Seismological Society of America, 72, 1167-1183.

Zhang, Z., Xu, J. & Chen, X., 2015. The supershear effect of topography on rupture dynamics, Geophysical Research Letters, 43, 1457-1463.

Andrews D.J, (1976), Rupture propagation with finite stress in antiplane strain, J. Geophys. Res. Solid Earth, 81, 3575-3582

Barall, M., (2009). A grid-doubling technique for calculating dynamic three-dimensional rupture on an earthquake fault, Geophysical Journal International, 178, 845-859, doi:10.1111/j.1365-246X.2009.04190.x.